Available online at www.sciencedirect.com

ScienceDirect

journal homepage: www.elsevier.com/locate/he

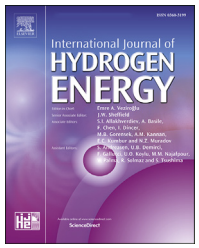

Hydrogen direct reduction and reoxidation behaviour of high-grade pellets

Pasquale Cavaliere [a,*], *Leandro Dijon* [b], *Aleksandra Laska* [c], *Damian Koszelow* [d]

[a] *Department of Innovation Engineering, University of Salento, Via per Arnesano, 73100, Lecce, Italy*
[b] *VALE, Route de Pallatex 29 St-Prex, 1162, Losanna, Switzerland*
[c] *Faculty of Mechanical Engineering and Ship Technology, Gdansk University of Technology, Narutowicza 11/12, 80-233, Gdańsk, Poland*
[d] *Advanced Materials Centre, Faculty of Electronics, Telecommunications and Informatics, Gdańsk University of Technology, 80-233, Gdańsk, Poland*

HIGHLIGHTS

- High grade pellets were direct reduced through hydrogen at high pressure.
- Porosity is reduced by a maximum of 15% after reduction.
- The kinetics of reduction depends on the composition and porosity of the pellets.
- Reoxidation resulted slow up to 500 °C in air.
- A remarkable acceleration of the reoxidation was recorded at 600 and 700 °C in air.

ARTICLE INFO

Article history:
Received 4 July 2023
Received in revised form
8 August 2023
Accepted 21 August 2023
Available online 01 September 2023

Keywords:
Direct reduced iron
Hydrogen
Porosity
Metallization
Reoxidation

ABSTRACT

High grade pellets with basicity index close to 0.5 were directly reduced in pure hydrogen atmosphere. The reduction experiments were performed in the temperature range 800–1000 °C at the pressure of 8 bar. The pellets internal structure was analysed through micro tomography observations in the unreduced and reduced conditions. After reduction, the pellets showed a variation of porosity up to more than 15% with a remarkable change in the pore dimensions and aspect. Given the pores aspect variations, tortuosity strongly varied. This is believed to have large influence on the pellets reduction kinetics depending on the reduction conditions. After reduction, the pellets were re-oxidized in the temperature range 200–700 °C for different times. Up to 500 °C the weight increase due to oxidation resulted very slow, for higher temperatures the re-oxidation behaviour showed a very remarkable acceleration.

* *Corresponding author.*
E-mail address: pasquale.cavaliere@unisalento.it (P. Cavaliere).

https://doi.org/10.1016/j.ijhydene.2023.08.254

1. Introduction

To obtain primary iron, there are essentially two production routes which are technically and commercially viable: reduction in blast furnaces, whose product is liquid, called pig iron, and the direct reduction process (taking place in the solid state) where the product is known as sponge iron, or DRI (direct reduced iron) [1,2]. Therefore, DRI is a generic term used for metallized products through reduction of iron ore in solid state (granules and pellets) in direct reduction reactors. It consists mainly of metallic iron, residual iron oxides (which do not were fully reduced in the reactor) and typical minor compounds such as silica, alumina, calcium. DRI re-oxidation is a crucial well-known phenomenon all over the world, mainly in the stages of storage and transoceanic transport [3]. Re-oxidation is characterized by some features that could favour self-ignition, which can bring risk conditions and even lead to serious accidents in the reduced material handling; water cannot be used in extinguishing fire caused by reoxidation [4]. Industrially, some pellets generate DRIs with a greater tendency to the phenomenon of self-ignition [5]. Parallel to this fact, the conditions of the direct reduction process also were changed when working with such loads, leading to believe that these materials behave differently from the others inside the reactor [6]. In addition, after the direct reactor processing, pellets can remain for different times at high temperature before electric arc furnace melting; given this, re-oxidation can lead to material wasting in a remarkable percentage. Despite these characteristics observed in direct reduction process, the currently existing and ISO standardized laboratory test methodologies do not reflect this behaviour and they do not provide information in the sense of predicting the occurrence of autoignition [7]. During direct reduction, iron oxides are reduced to metallic iron in the solid state, without the occurrence of a melting step [8]. Macroscopically, the physical appearance of sponge iron is similar to the material fed (pellets or granules), except for the significant increase in porosity and generation of fines [9]. Chemically, the oxygen bounds are removed leaving a very porous structure [10]. Both raw materials and reduction temperature can influence the porosity of the produced DRI [11–13]. The extremely porous structure contributes to reoxidation reactions, the main factor that led sponge iron to be considered a hazardous material for handling and transport [14]. Several accidents were reported on ships that needed to be unloaded in a hurry due to the self-heating of the charge. There are also a number of reports of piles of burning storage in several plants around the world [15]. Nowadays the ships carrying DRI have inertization systems for the holds and passivation of the cargo, reducing to zero the accident risks. Inertization consists of reducing the activity of metallic iron [16]. DRI reoxidation mechanisms can be simplified into two distinct processes: corrosion in aqueous medium and air oxidation [17]. While dry oxidation occurs slowly at low temperatures, the reaction aqueous water develops rapidly and can be considered as the cause of increased temperature to levels at which oxidation reactions at high temperatures begin to occur at high speeds and become self-sustaining. Thermal conductivity values as well as the self-ignition temperature of DRIs are considered low, therefore the low heat dissipation will make it possible to achieve more easily the ignition temperature [18]. The autoignition temperature can be defined as one in which the metal will oxidize very quickly, promoting a sharp increase in temperature, which may be accompanied by the appearance of flames [19,20]. The pyrophoric behaviour of sponge iron is caused by its inability to dissipate heat of oxidation leading to an increase in temperature [21]. The heat generated by the exothermic reactions is approximately 4.07 kcal/g of absorbed oxygen. Thus, the absorption of 0.1% of oxygen in sponge iron can mean an increase of 35 °C under adiabatic conditions. This heat will not be dissipated due to the low thermal conductivity of the material. This also increases the speed of oxidation that will further raise the temperature of the DRI [22]. The autocatalytic process continues until spontaneous ignition occurs. The dissipation is controlled by temperature and by other factors such as geometry and storage form. Reoxidation is also influenced by the prior direct reduction experienced by the pellets [23]. This is due to the fact that higher temperatures lead to an increase in the sintering rate causing coalescence of micropores and growth of macropores, reducing the surface area, contributing to the reduction of DRI reactivity [24]. One of the main reasons for this behaviour is due to the rapid reduction in porosity due to closure of the entrances to the interconnected network of pores during oxidation. This behaviour is much more pronounced in the case of hydrogen direct reduction given the faster reduction behaviour with respect to carbon monoxide atmosphere. A fraction of intragranular voids decreases (due to the difference in volume between metallic iron and their oxides) thus reducing the diffusion of the oxidizing gas, as well as the particle surface reactivity [25]. The rate of oxidation is then reduced due to the blockage of the non-porous oxide layers, when the inner grains become isolated from the interconnected network and the transport of reagents occurs only through diffusion in solid state [26]. DRI reactivity, i.e., the tendency of a reduced material to react with oxygen of air causing reoxidation, depends on the raw material, the direct reduction process and the operating conditions of the reduction reactor [27]. Pellets with higher iron content and a higher degree of metallization have lower ignition temperatures [28]. The porosity and pore size in the external surface of the DRI have great influence on its reoxidation behaviour [29]. Hydrogen reduction produces smaller pores for the same reaction conditions. The gas flow also has a significant impact on the pore size – the lower the flux, the larger the pores result [30]. Anyway, the carbon absence during reduction does not allow the formation of cementite content formed on the surface of the DRI. The formation of cementite reduces the metallic iron activity, making the DRI more stable [31]. Given all this, some scientific evidences are presented in literature on the re-oxidation behaviour of pellets reduced in carbon atmosphere or mixed CO + H2 atmospheres. To the best authors knowledge, no detailed informations are provided on the detailed porosity

behaviour as a function of reducing temperatures and microstructural issues and on the consequent reoxidation behaviour.

The aim of the present paper is the analyses of reoxidation of high-grade pellets reduced by hydrogen at different temperatures and high pressure.

2. Experimental procedure

The pellets analysed in the present study were provided by VALE (Brazil). The iron ore pelletizing plant begins with the grinding process, where the ore is mixed with a specific solid content and grinding balls of varying sizes. The plant has multiple ball mills, each with a considerable capacity to process the ore. The quality parameter during this stage refers to the Specific Surface (blaine), with a usual target ranging from 1500 to 1,600 cm^2/g. Once the grinding is completed, the material undergoes vacuum filtering. The filters used in this process are large in diameter and provide a significant filtering area. After the filtering stage, the material is subjected to High Pressure Grinding Rolls (HPGR), which further refines the quality parameters. The HPGR process has a notable capacity and uses rolls with specific dimensions in diameter and width.

Finally, the material is sent to the pelletizing discs, which have a wide range of capacities per disc. The plant features multiple discs, with both discs and screens having specific dimensions in diameter and width. Then the material is subjected to the endurance processing. Finally, the pellets are filtered in order to eliminate fines (<5 mm). The pellets were reduced in hydrogen atmosphere at the gas pressure of 8 bar and temperatures in the range 800–1000 °C. In both single and multi-pellets reduction experiments, the reactor is equipped with a load cell measuring the weight variation during the reduction process.

From the reduction curves (reduction percentage vs. time to reduction) they were calculated the kinetics constants and the rates of reduction.

The kinetic constant was calculated through the three dimensional diffusion model (Eq. (1)):

$$k = \frac{\left[1-(1-\alpha)^{\frac{1}{3}}\right]^2}{t} \quad (1)$$

And through the three dimensional phase boundary controlled reaction (Eq. (2)):

$$k = \frac{1-(1-\alpha)^{\frac{1}{3}}}{t} \quad (2)$$

where α is the fraction reacted (0–1) and t is the time at which a given fraction of the material reacts.

The reduction rate is analysed through the definition of two indexes described in Eqs. (3) and (4):

$$\frac{dR}{dt}_{40} = \frac{33.6}{t_{60}-t_{30}} \quad (3)$$

$$\frac{dR}{dt}_{90} = \frac{13.9}{t_{95}-t_{80}} \quad (4)$$

with t_{95}, t_{80}, t_{60} and t_{30} being the time required to reduce the pellets by 95, 80, 60 and 30%.

A scanning electron microscope Zeiss EVO 40 equipped with microanalyses was employed for the surface characterization and for the microstructure evolution observations of pellets before and after the reduction experiments. The pellets pores aspect and evolution were analysed by microtomography by employing a Phoenix v/tome/x s (General Electric). X-ray computed microtomography is a non-destructive technique that allows the internal and three-dimensional visualization of a sample subjected to a source of ionizing radiation with virtually no need for physical and chemical preparations of the pellet. It is based on the same principles as conventional radiography, where each part of a sample absorbs the rays differently. In this way, it is possible to study the two-dimensional cross sections in a non-destructive way and through mathematical principles, it is possible to reconstruct them in order to build the respective three-dimensional model of the sample, allowing thus the visualization and quantification of the internal structure of the material. Computed tomography produces an image very close to the reality by displaying the average attenuation of each small volume element, ordering the beam attenuation information and translating the information quantitatively [33–35]. After the post-processing step, the image finally goes to the attribute extraction in which the quantitative data of interest are obtained. It is possible to understand and evaluate the numerical data from the image and later it is possible to proceed to a classification stage and pattern recognition. Pore segmentation was performed with the help of free software FIJI/ImageJ. A lower limit was visually determined where some pores were not selected, and an upper limit, where pores that have not been previously filled can be selected. The threshold (maximum or minimum) can be fixed for all sample layers. Determining the threshold is important because has a great impact on obtaining the porosity percentage of iron ore pellets.

The microtomography data were analysed with Image J software for the characterization of the porosity behaviour of the pellets. Selected reduced pellets were reheated in a heat treatment resistance furnace in the temperature range 200–700 °C for different times in order to analyse the reoxidation behaviour.

3. Results and discussion

The aspect of the pellets before reduction is shown in Fig. 1.

The pellets mean diameter ranged from 1.14 to 2 cm. We indicate in the following small size pellets those with a mean diameter between 1.14 and 1.3, medium size pellets those with a mean diameter between 1.3 and 1.6 cm and big size pellets those with a mean diameter larger than 1.6 cm.

The pellets pores mean diameter varied from 4.5 to 2.0–8.5 μm for the small, medium and big pellets respectively. So, with the same pelletizing procedure porosity decreases and then increases again as the mean pellet diameter increases.

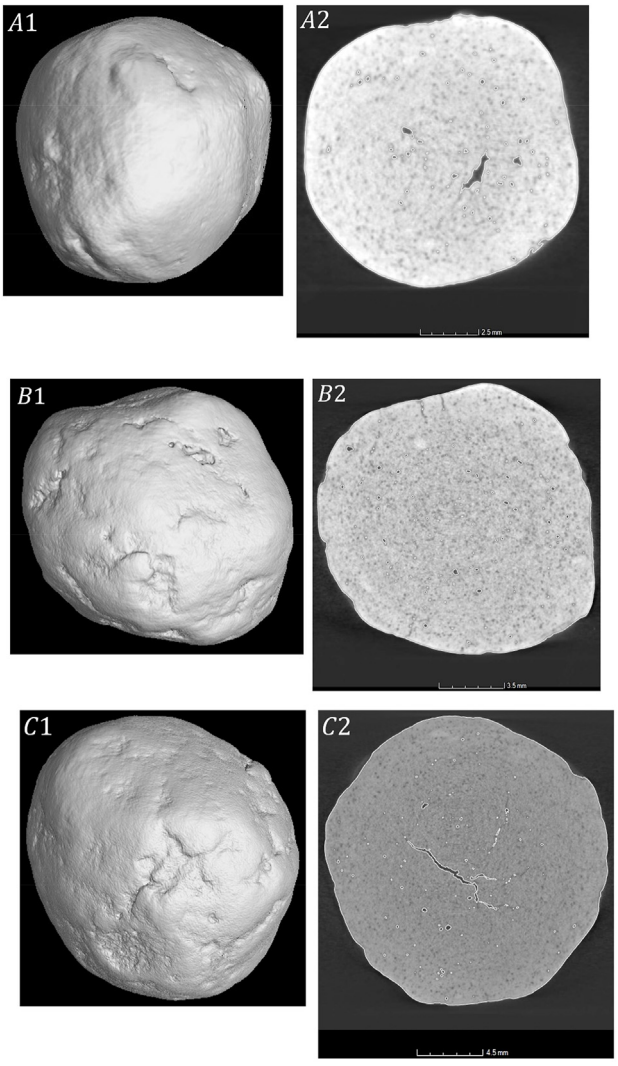

Fig. 1 – Microtomography aspect and cross section porosity of the analysed pellets A1 and A2 small pellet, B1 and B2 medium pellet, C1 and C2 large pellet.

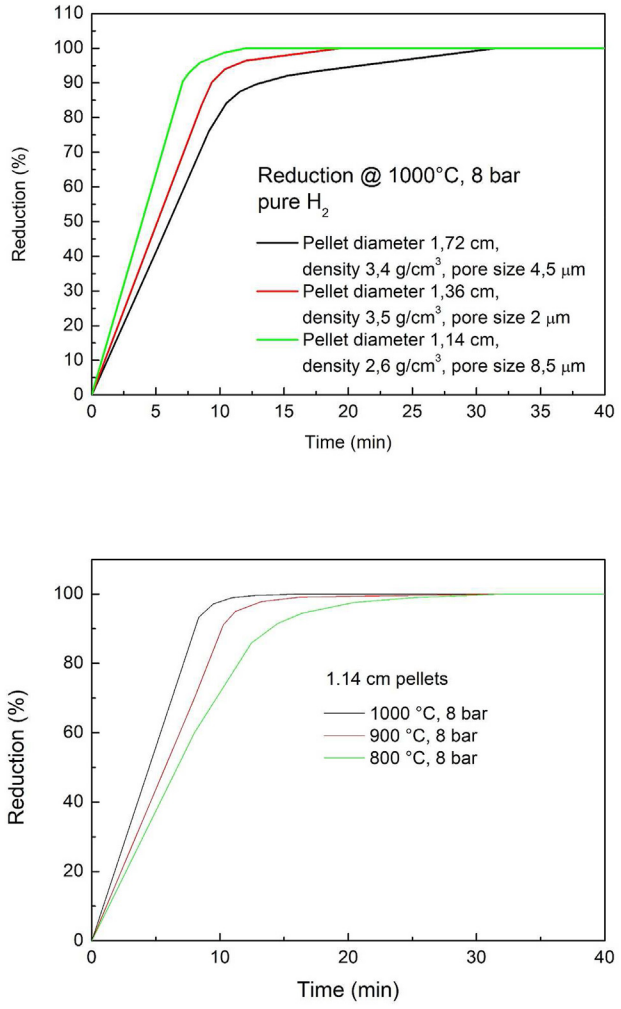

Fig. 2 – Reduction curves for different pellets at 1000 °C and 8 bar in hydrogen atmosphere a); small pellets reduction at different temperatures b).

Porosity is generally the rate limiting step of the reduction process. The main factor influencing the process is the pellets porosity in terms of dimensions, tortuosity and pores distribution. This is related to the specific hydrogen volume reacting with the pellet internal surface [36]. This is why, in the case of low porosity and low surface pores dimensions, the gas finds many obstacles to penetrate inside the pellet [37]. In this case, the solid state diffusion from the surface starts to become more important but it results different orders of magnitude slower than the gas diffusion. So, all the chemical reactions are driven by the hydrogen adsorbed at the pellet surface [32].

This was consistent with the performed compression strength measurements of the pellets varying from 3.5 to 5 to 4.5 kN for the small, medium and big pellets respectively. This aspect is fundamental for the swelling behaviour of the pellets in the industrial reactors [38,39]. In fact, porosity largely influences the direct reduction kinetics and as it is decreased because of the pellets compression inside the DRI reactors, the time to complete reduction is largely delayed.

An example of the reduction curves in the experimented conditions is shown in Fig. 2.

The time to reduction is inversely proportional to the pellet diameter even if the overall behaviour is also related to the porosity and pores dimensions.

As a matter of fact, Fig. 3 shows the results of the reduction behaviour as a function of temperature and pores size for the studied high-grade pellets [40].

Given the time to reduction, the factor most influencing is the pellet diameter. This is also related to the density and the reducing atmosphere. In addition, it was observed that as the diameter of the pellet changes, the influence of density varies. If the pellet has a high density, the pellets' diameter effect decreases, the contrary is revealed in the case of large particles for which the effect of the density is reduced. Time to reduction is both related to the absolute porosity but also to the surface pores dimensions. The larger these pores are, the faster the pellets can reduce. This is obviously dependent on the pellet density describing the behaviour of pores in the pellets bulk, in fact, as the pellet density increases the time to reduction increases.

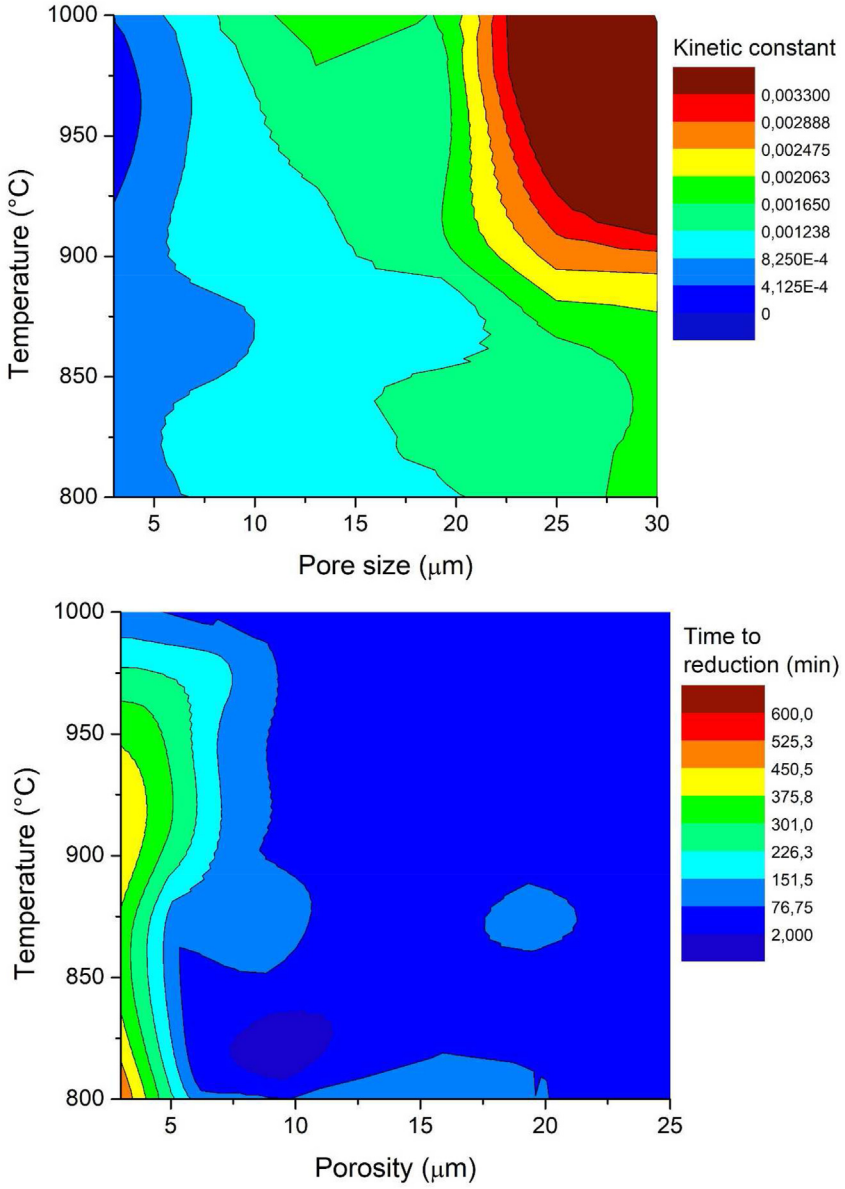

Fig. 3 – Kinetic behaviour a) and time to reduction b) as a function of porosity and temperature for the high grade studied pellets.

It is clear how the kinetic of the reduction is largely accelerated as the pores dimension increases for all the temperatures. So, the larger the pores are, the faster the pellets reduce. In the case of high pellets density the reactions of reduction are known to evolve stepwise that can be modelled through a shrinking core description [41]. In the case of low density pellets, the gas diffuses very fast and the reduction times are significantly reduced. So, the time to reduction is lower for all those pellets with low density that in this particular case are also characterized by an intermediate surface pores dimensions. By observing the behaviour of the pellets reduction in terms of the kinetic constant variations, in the case of hydrogen direct reduction a hierarchy of phenomena can be underlined all determining the overall reduction in the time and space domains. The phenomena developed in an industrial shaft furnace, in fact, depend on the kinetics behaviour and on the heat and mass transfer from the macroscopic scale to the atomic one (in different times) involving catalytic processes, diffusion, dissociation up to transfer of charges. In addition, these phenomena are characterized by a non-linear interplay among them. This needs the employment of very different characterization and modelling instruments to be addressed. So, the macroscopic gas transportation and diffusion plays different roles at different scales of the process that is strictly related to the pellets microstructure and chemical-physical properties. Al microscale, the process kinetics are determined by both micro and atomic scale phenomena because of the different oxides involved transformations, of the crystal defects and of the local compositions.

After reduction, the aspect of all the pellets is remarkably varied in terms of pores aspect, dimensions and geometry (Fig. 4).

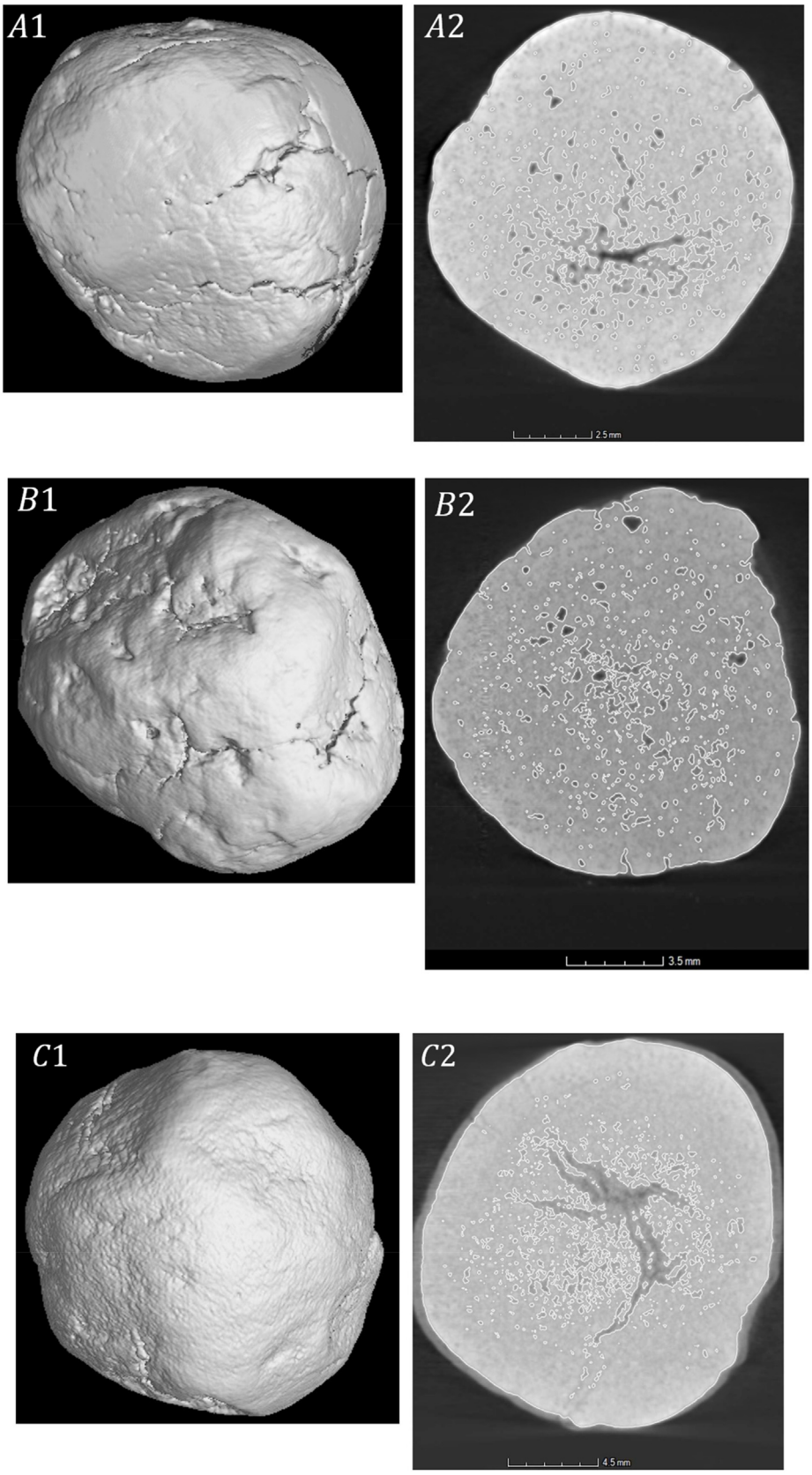

Fig. 4 – Tomography aspect of the studied pellets after reduction A1 and A2 small pellet, B1 and B2 medium pellet, C1 and C2 large pellet.

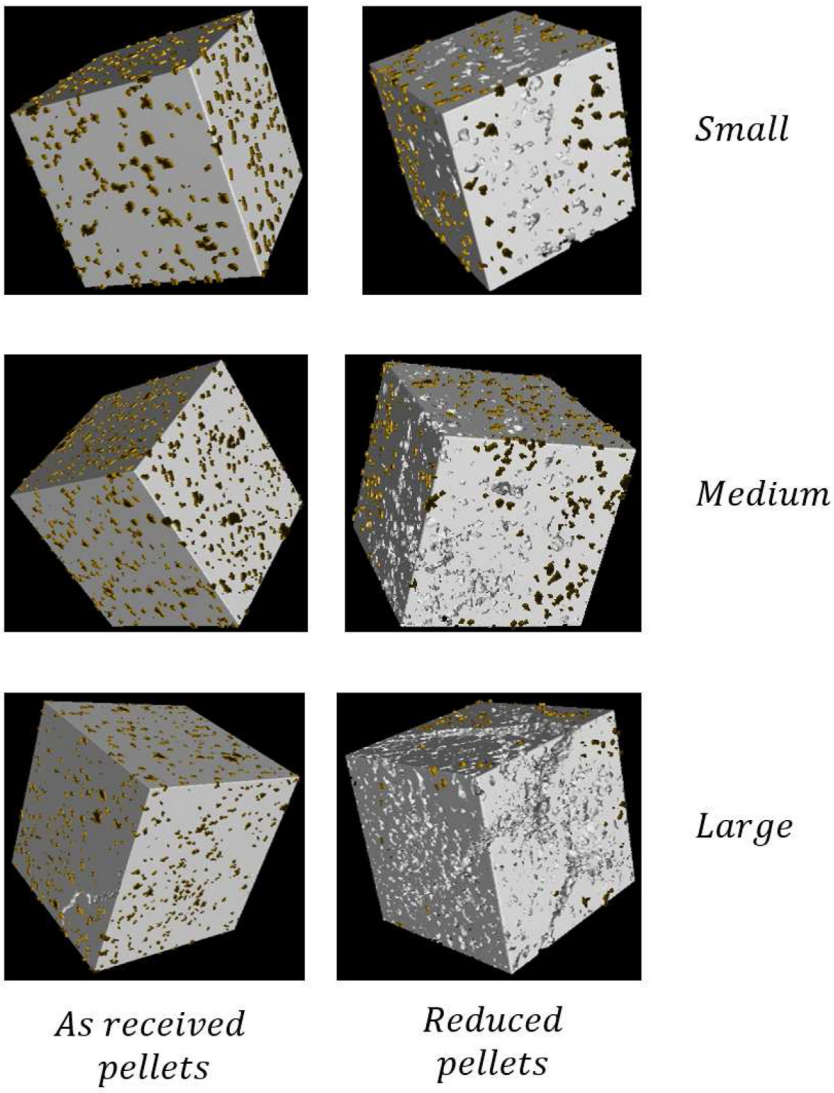

Fig. 5 – Selected volumes of the pellets before and after hydrogen reduction.

The images have a contrast well defined, which allowed a better segmentation of the cutting tone. In order to differentiate between open and closed porosity, a new pore discrimination methodology based on the calculation of the Euclidean Distances (EMD) to be able to delimit the edge of the pellet was applied (Fig. 5).

The EMD of the filled object provides a tonal reference, in which each object has a tone associated with the distance from the pixel to the edge of the object and the minimum that refers to the connected pores, since this type of pore is in contact with the edge. Therefore, after calculating of the EMD, there is the construction of a graph of minimum intensity where the smallest values refer to the connected pores (Fig. 6).

The segmentation was done interactively, with the choice of a fixed threshold for all 2D layers of the samples. The cutoff tone value for segmentation changes the amount of pixels that are measured. To obtain the percentage of pores, verifying that the images of iron ore pellets even after all preprocessing previously explained, are still difficult to segment, we chose 5 values of segmentation thresholds, with a difference of 5 tones between them, for each sample. Then, for each volume generated from the segmentation with these values, pore volume was extracted. Thus, the estimated porosity values of each sample are within a range determined by these threshold values [42].

The cut-off value for the distinction of pores between open and closed ones is done manually. This can lead to measurement errors and it would be interesting to conduct a study so that the threshold is automatically defined in future analyses [43,44]. In the results obtained for the whole pellet, the percentage of open and closed porosity in relation to the total pores can be calculated [45]. Here it can be seen the presence of large areas in the reduced pellet that corresponds to connected pores (Fig. 7).

The presented results clearly indicate that the specific surface decreases as that the reduction temperature is increased. This behaviour is due to the fact that migration occurs in the solid phase at high temperatures. This causes an increase of the total pore volume while the small pores between the particles disappear, reducing the specific surface of

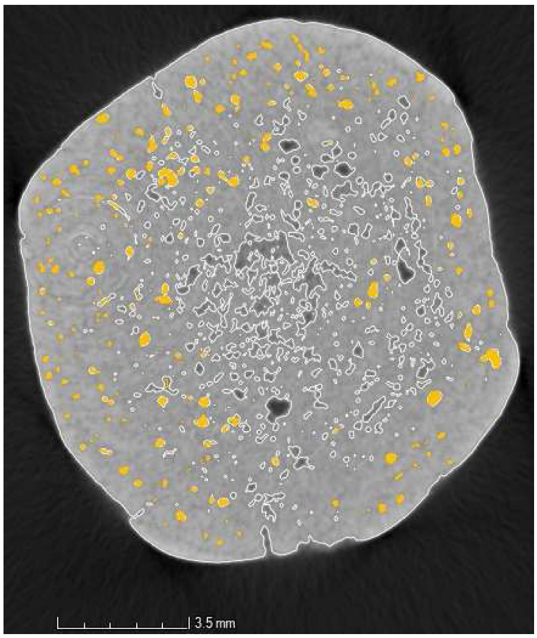

Fig. 6 – Example of pores detection in the medium size pellet reduced at 950 °C.

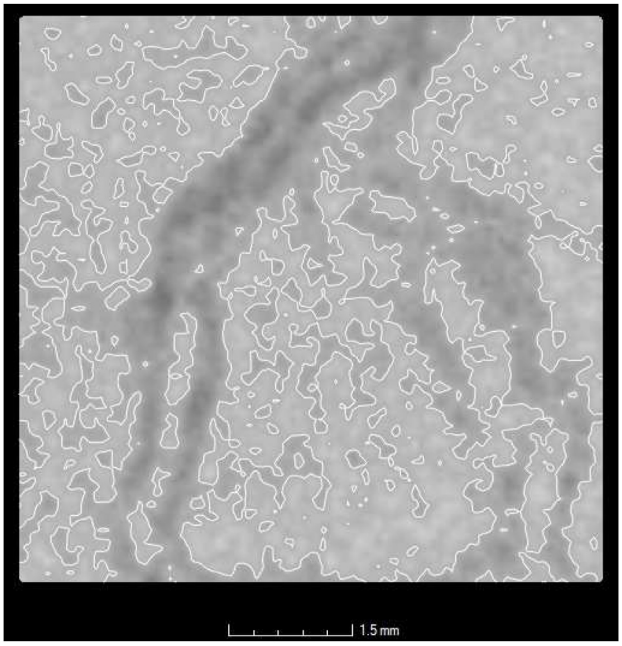

Fig. 7 – Connected pores in the larger pellet reduced at 950 °C.

the material [46]. An excess of the reduction temperature increase leads to pore sintering with fast reduced porosity. Porosity increases by around 15% for all the pellets size as shown in Fig. 8.

Porosity tends to increase as the reduction processes take place. This phenomenon tends to lead to an acceleration of the reaction kinetics as the reduction process advances. Given

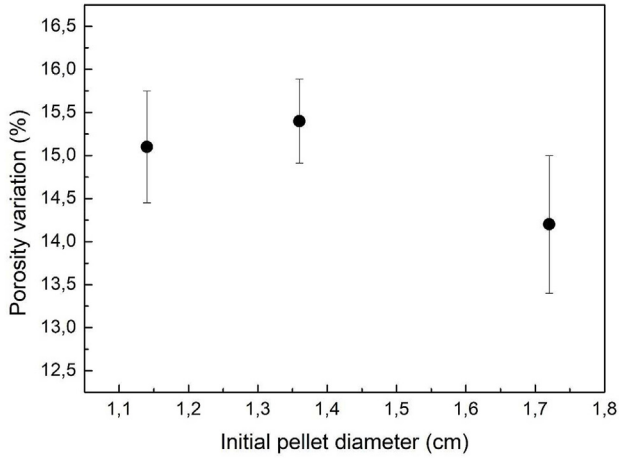

Fig. 8 – Porosity variation after hydrogen reduction for the pellets with different starting diameter.

that the diffusion can be the rate-limiting step, porosity and pores dimensions have a remarkable influence on the reduction process [47]. This is due to the fact that both porosity and pores size influence the specific area of the pellets then defining the available surface for the reactions development. This aspect is crucial and must be precisely defined in a model that would soundly describe the evolution of these systems.

Entropy generation has two main contributes from the chemical reactions and from the mass transfer. By considering the entropy generation contributions as separate, as the porosity in the pellet decreases the entropy generation due to heat transfer increases. Here, the entropy increases immediately during the first stage of reduction because of the temperature gradient between the pellet surface and the heated hydrogen. After this, entropy decreases up to a steady state and it remains constant because the thermal gradient tends to decrease as the reduction process proceeds.

By considering pellets where the porosity increases, the resistance to the gas penetration inside the pellets decreases. As a consequence of the easy gas penetration, the entropy generation decreases. The second contribution is the entropy generation due to the chemical reactions. Here, the entropy generation tends to rapidly increase in the first reaction stages but in this case it decreases up to a zero value as the chemical reactions proceeds. Also in this case, as the porosity of the pellets increases, the entropy generation decreases. Obviously, the entropy generation leads to increased energy expenses for the overall reduction process [48].

The other contribution to the entropy generation comes from the mass transfer. This contribution shows a fast increase in the first stages of reduction and then it decreases up to a plateau value. In the case of high porous pellets, this contribution can approach the zero value after the peak increase because of the reduction to the gas penetration inside the pellets. Anyway, the entropy is never null because of the compositional gradient between the pellet surface and the not already reduced bulk. To give an idea of the total contribution, we can say that the highest effect is due to the heat transfer,

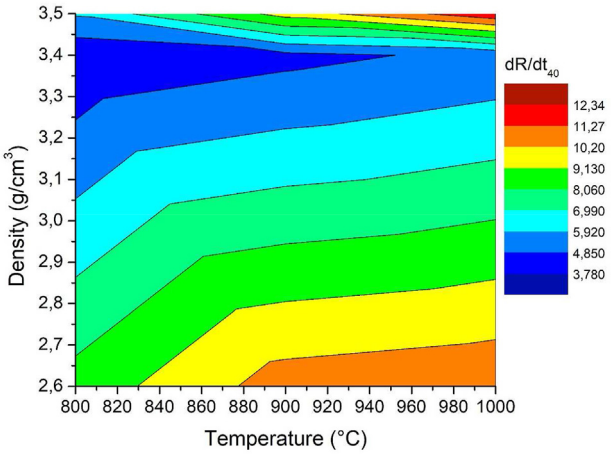

Fig. 9 – dR/dt40 index as a function of reducing temperature and pellets density.

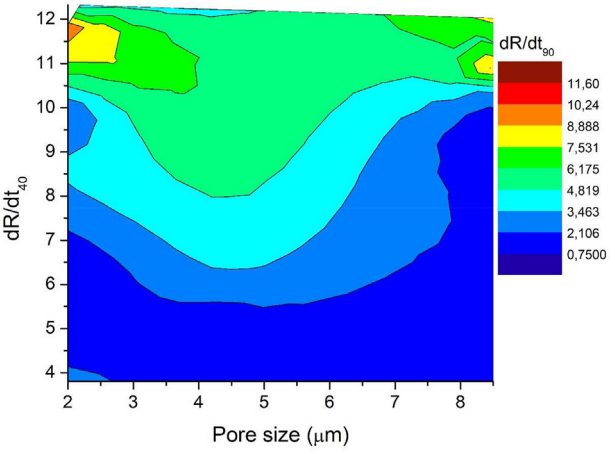

Fig. 10 – dR/dt_{90} index variation as a function of the surface pore size and the dR/dt_{40} index.

an intermediate effect is due to the chemical reactions while the lowest effect is due to the mass transfer [49,50]. So, during the initial stages of reduction the process is controlled by both the chemical reaction and the gas diffusion while in the second stage of reduction the rate limiting step is the interfacial chemical reactions [51].

The first stage (rapid) of reduction is generally evaluated through the calculation of the dR/dt40 index [11]. Here, it is strongly dependent on the pellets density as shown in Fig. 9.

In the case of very small surface pores and then a denser surface (medium size pellets), a very hard iron layer form on the surface. If this very hard dense iron layers develop during reduction this strongly tends to lower the reduction rate [52]. This, in fact, limits the gas penetration inside the pellet by reducing the effect of the hydrogen. In the case of very hard layers rapidly formed on the surface the reactions tend to be governed by the solid-state diffusion. The gas penetration through the hard iron layers can be improved at higher levels of temperature [53]. The inconvenience is due to the softening of the pellets as the temperature increases. This can reduce the pellets porosity by consequently reducing the reduction rates. Obviously, this also influences the final reduction step of the overall process normally evaluated through the dR/dt_{90} index as shown in Fig. 10.

The different dependence on the pellets properties and on the processing parameter is due to the fundamental aspect that they refer to different transformations taking place at different reduction steps (different oxides reduction) and to the fact that the material composition and pellets shape tends to vary as the reduction process is carried out [54]. So, the two indexes are indicative of how the reduction of the different iron oxides are going to be reduced condition by condition. So, the dependence of the single index on the different processing parameters changes. The different stages of reduction indicate the behaviour of different reactions taking place in the pellet, so, the absolute values and the influence of the input parameters vary. Generally, the pore size is very influencing the dR/dt_{40} index and it has lower influence on the final stages of reduction [55]. This is due to the not-negligible aspect that the pores dimension and pores geometry tend to modify as the reduction proceeds. So, in the final stages of reduction the pores from which the gas continues to penetrate the pellet are different from the beginning of the process. By considering the entropy generation and then the energy consumption, the peak is reached with inverse proportionality to porosity and pores size. After this, pores tend to increase in dimension and then the entropy generation decreases. So, also the energy consumption tends to decrease as the pores dimensions vary by going from dR/dt_{40} to dR/dt_{90}.

The data belonging to different temperature conditions for various pellets size are shown in Table 1.

So, porosity increases, the single pore dimension increases and also the pores tortuosity varies. As a matter of fact, the tortuosity of pores for the small size pellets reduced at 950 °C in pure hydrogen is shown in Fig. 11.

The same behaviour can be underlined for the large size pellets as shown in Fig. 12.

So, tortuosity tends to continuously vary during the reduction. Its starting value and the variation during the reduction influences the pellets kinetics. As a general behaviour, the reduction kinetics as a function of temperature and pores tortuosity is shown in Fig. 13.

So, for the same temperature tortuosity retards the reduction behaviour. It is intuitive to understand that, as the tortuosity increases, turbulence of the gas flowing inside the pores increases. In these conditions, the reduction rate tends to decrease [56]. Taking into account the tortuosity factor inside the pellets, the time to reduction increases as the tortuosity of the pores increases, as the porosity decreases (increased density) and the pores dimensions decrease. This is why from the energy point of view, these parameters largely lead to variations in the entropy generated during all the reduction phases [57]. Entropy starts to increase in the first stages of the direct reduction as a consequence of the heat transfer between the heated hydrogen and the pellets surface. The entropy tends to increase as the porosity and the gas ration decrease because of the reduction of the exchange surfaces. The entropy generation is then further increased as the pores tortuosity increases. This is due to the fact that tortuosity is an obstacle for the gas flowing and for its ideal path inside the pellet. Basically, this

Table 1 – Mass variation of different pellets reduced through hydrogen atmosphere.

Temperature °C	Reduction time (min)	Initial diameter (cm)	Final Diameter (cm)	Initial mass (g)	Final mass (g)	Mass variation (%)
950	90	1,36	1,18	3,98	2,83	29
950	90	1,3	1,2	3,98	2,83	28,9
950	90	1,46	1,41	5,65	4	28,6
950	90	1,5	1,41	5,9	4,2	28,9
950	90	1,85	1,72	10,49	7,43	29,1
950	90	1,8	1,74	10,1	7,23	28,6
1000	90	1,37	1,17	4,08	2,88	29,36
1000	30	1,74	1,6	9,32	6,53	29,92
1000	30	1,62	1,51	7,83	5,56	29
1000	5	1,4	1,3	4,3	3,06	28,9
1000	5	1,4	1,3	4,3	3,1	28,8
1000	20	1,43	1,32	5	3,55	28,8
1000	20	1,29	1,15	3,68	2,6	28,95
1000	20	1,55	1,41	6,1	4,3	28,9
1000		2	1,87	13,7	9,76	28,9

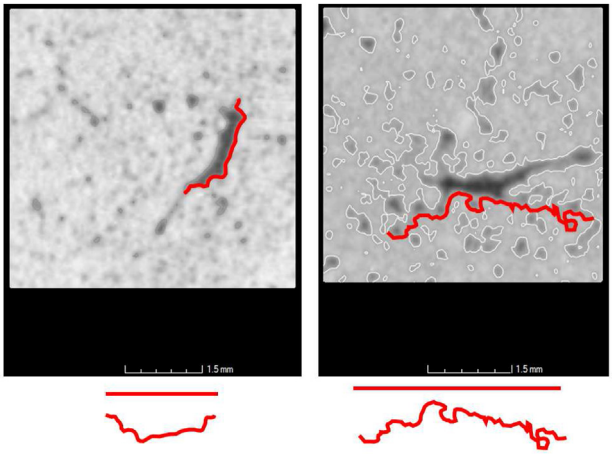

Fig. 11 – Cross section of the small pellets reduced before and after reduction at 950 °C.

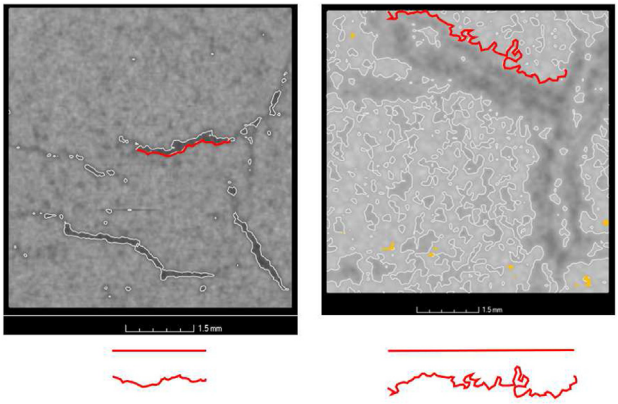

Fig. 12 – Cross section of the big pellets reduced before and after reduction at 950 °C.

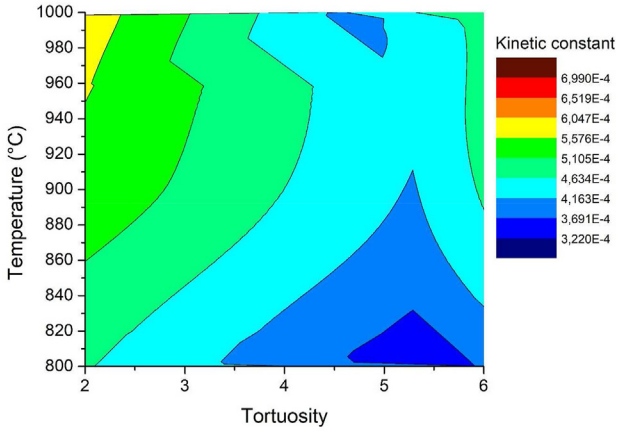

Fig. 13 – Kinetic behaviour of the pellets as a function of temperature and pores tortuosity.

reduces the overall gas diffusion and, as a consequence, its reduction effect. The tortuosity factor has also large implications of the overall entropy behaviour and then on the energy input during the direct reduction process [58]. In addition, the tortuosity is more influencing as the pellet diameter increases. Generally, as the tortuosity increases, the entropy generation and then the energy consumption increase. In addition, the entropy generation tend to increase with a non-linear behaviour especially in the final stages of reduction as the tortuosity of the pellets is very pronounced.

The microstructural analyses of the pellets evolution was performed through SEM and microanalyses. Fig. 14 shows the aspect of the large size pellets before reduction.

The composition measured through microanalyses is shown in Fig. 15 and the compositional data are listed in Table 2.

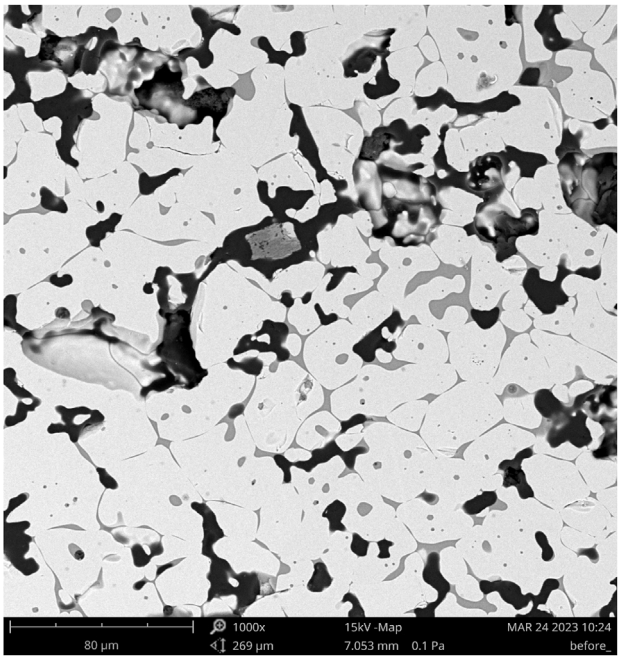

Fig. 14 – SEM micrograph of the as reived pellets.

The presented cross-section reveals a structure of well-connected particles of iron oxide before the reduction process. The porosity of the sample is also visible as black regions. It corresponds with the EDX element maps of iron and oxygen, where the lack of these elements overlaps the pores' regions. The microstructural analysis indicates that the iron oxide particles are surrounded by another oxide scale phase. The detailed EDX analysis of the cross section at higher magnifications (Fig. 16) revealed strong silicon and oxygen signals in these regions; thus, it seems that the dark grey phase can be assigned to silica.

Table 2 – Composition of the as received pellets.

Element Number	Element Symbol	Element Name	Weight Conc.
8	O	Oxygen	37.19
26	Fe	Iron	59.16
14	Si	Silicon	1.52
20	Ca	Calcium	1.17
13	Al	Aluminium	0.70
12	Mg	Magnesium	0.26

Based on our previous studies [11], the basicity index is optimal for the acceleration of the reduction reactions. The behaviour of the reduction seems to be related to the basicity index in a complex way. Some experimental evidences show how the reduction kinetics tend to increase as the basicity index varies from 0 to 1 and then it starts to decrease again as the basicity index increases. So a parabolic behaviour can be described for the time to reduction as a function of the basicity index. So again, the reduction behaviour of the industrial pellets is related to the quality of the raw material influencing the process and obviously the quality of the final

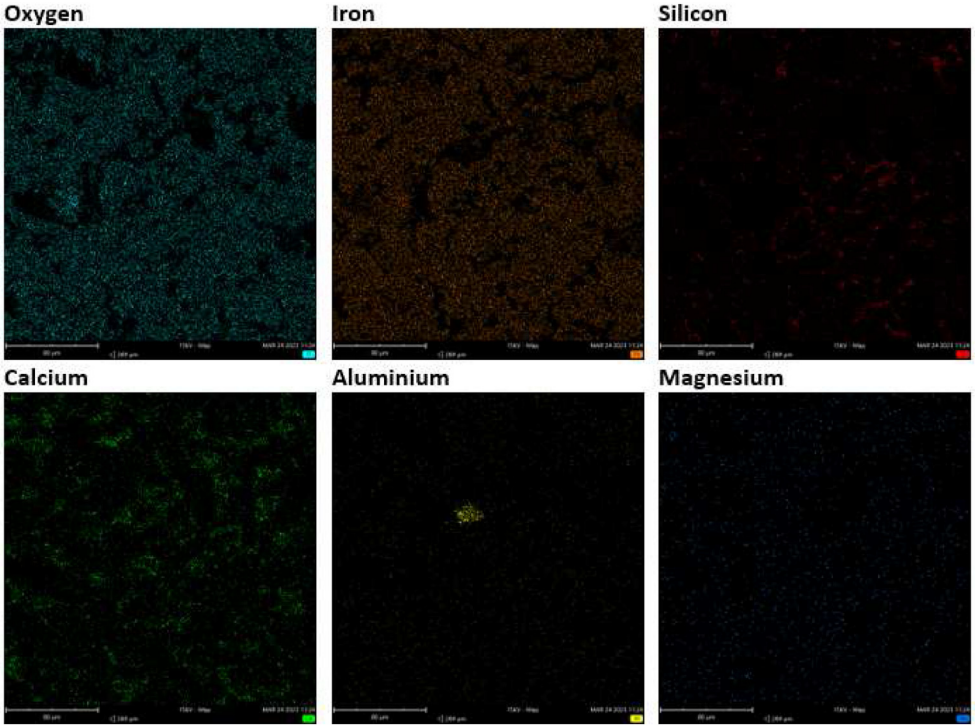

Fig. 15 – Compositional map of the as received pellets.

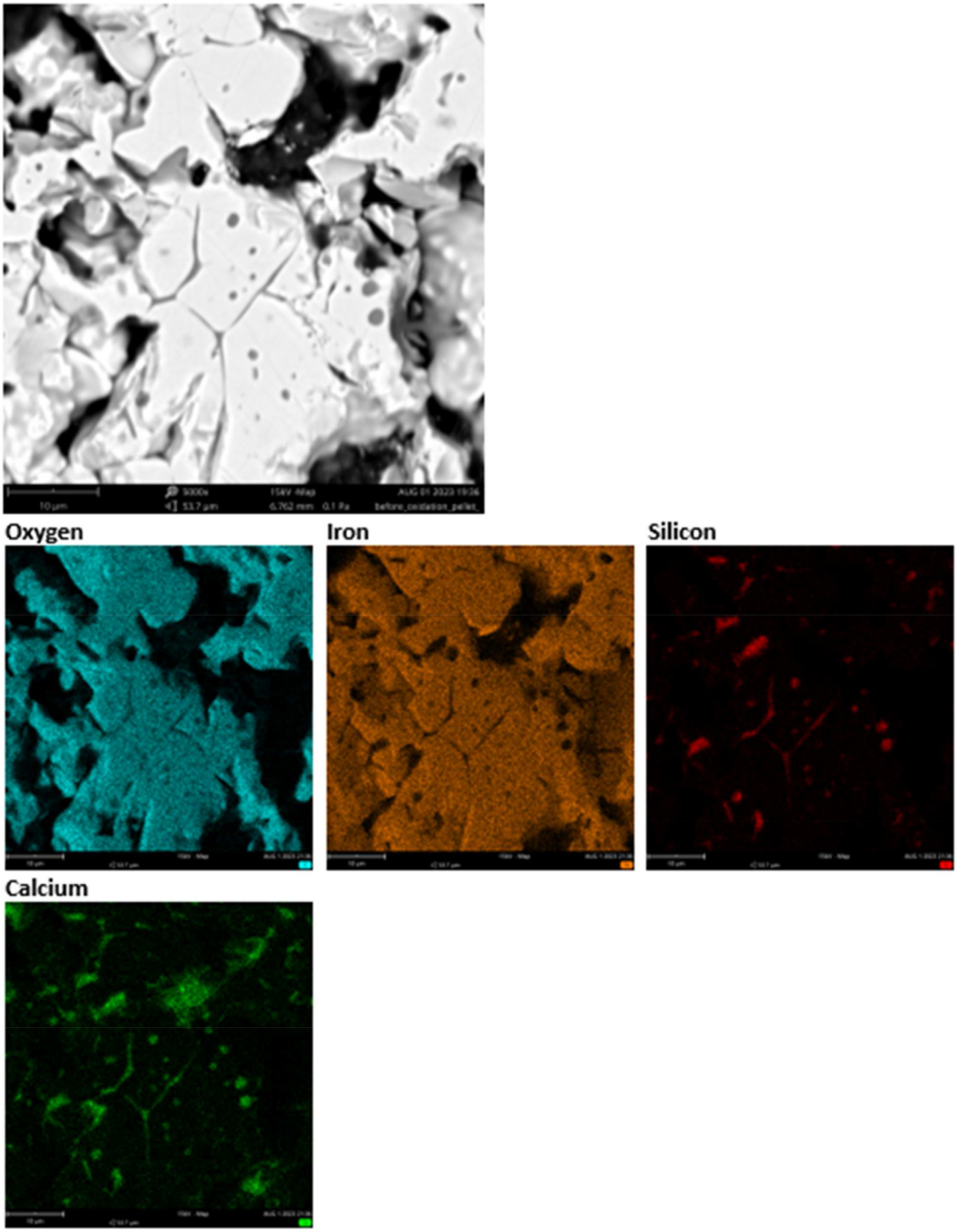

Fig. 16 – High magnification SEM and EDX maps of the unreduced pellets.

product to be employed for further operations. So, the basicity index should be retained at an appropriate level in order to optimize the reduction process of the pellets. In general, this is more pronounced in the case of further increase of the presence of CaO in the pellets composition. This, in addition, can lead to excessive brittleness of the produced pellets leading to difficult handling in the further processing operations [59,60].

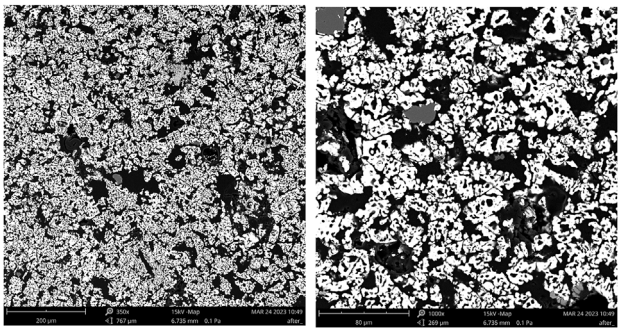

Fig. 17 – SEM micrographs at different magnification of the high grade pellet after reduction.

One can observe the predominance of hematite in all regions. There is also the local occurrence of Ca-ferrite, especially in the edge and outer mantle regions. It is observed an intergranular porosity, and medium pores probably coming from inputs. Calcium silicate permeates the interstices of the hematite particles.

After reduction at 950 °C the aspect of the pellets microstructure is shown in Fig. 17.

The composition measured through microanalyses is shown in Fig. 18 and the compositional data are listed in Table 3.

This is consistent with the metallization data calculated in different reduction conditions.

Table 3 – Composition of the pellet after hydrogen reduction.

Element Number	Element Symbol	Element Name	Atomic Conc.	Weight Conc.
26	Fe	Iron	63.25	95.27
14	Si	Silicon	7.74	2.11
20	Ca	Calcium	1.14	1.08
13	Al	Aluminium	0.85	0.54

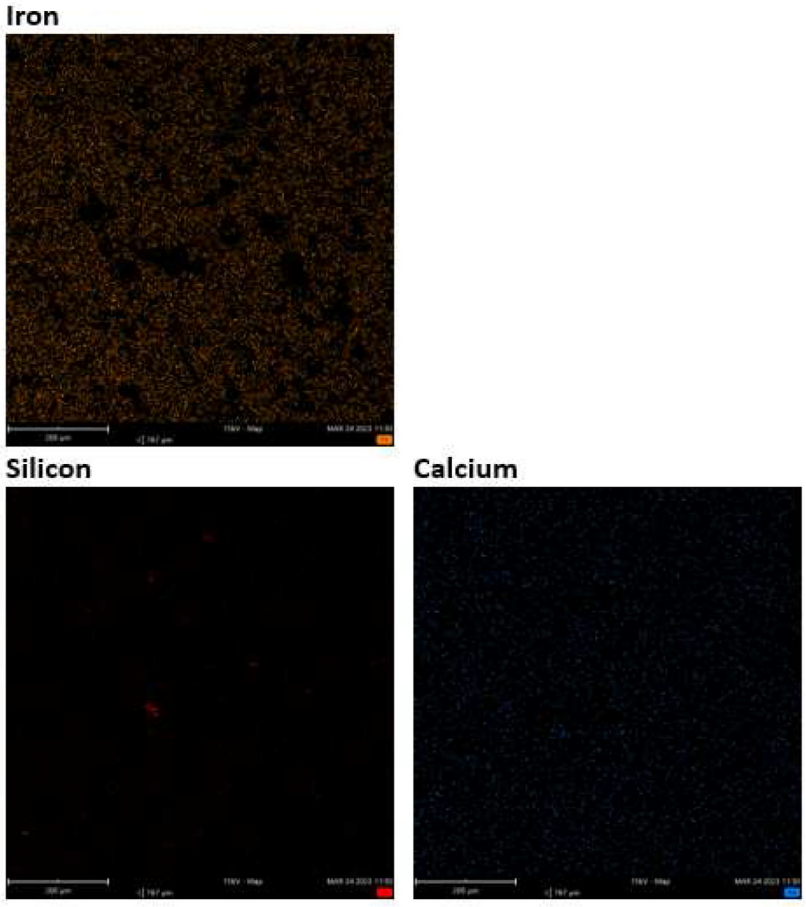

Fig. 18 – Compositional map of the pellets after hydrogen reduction.

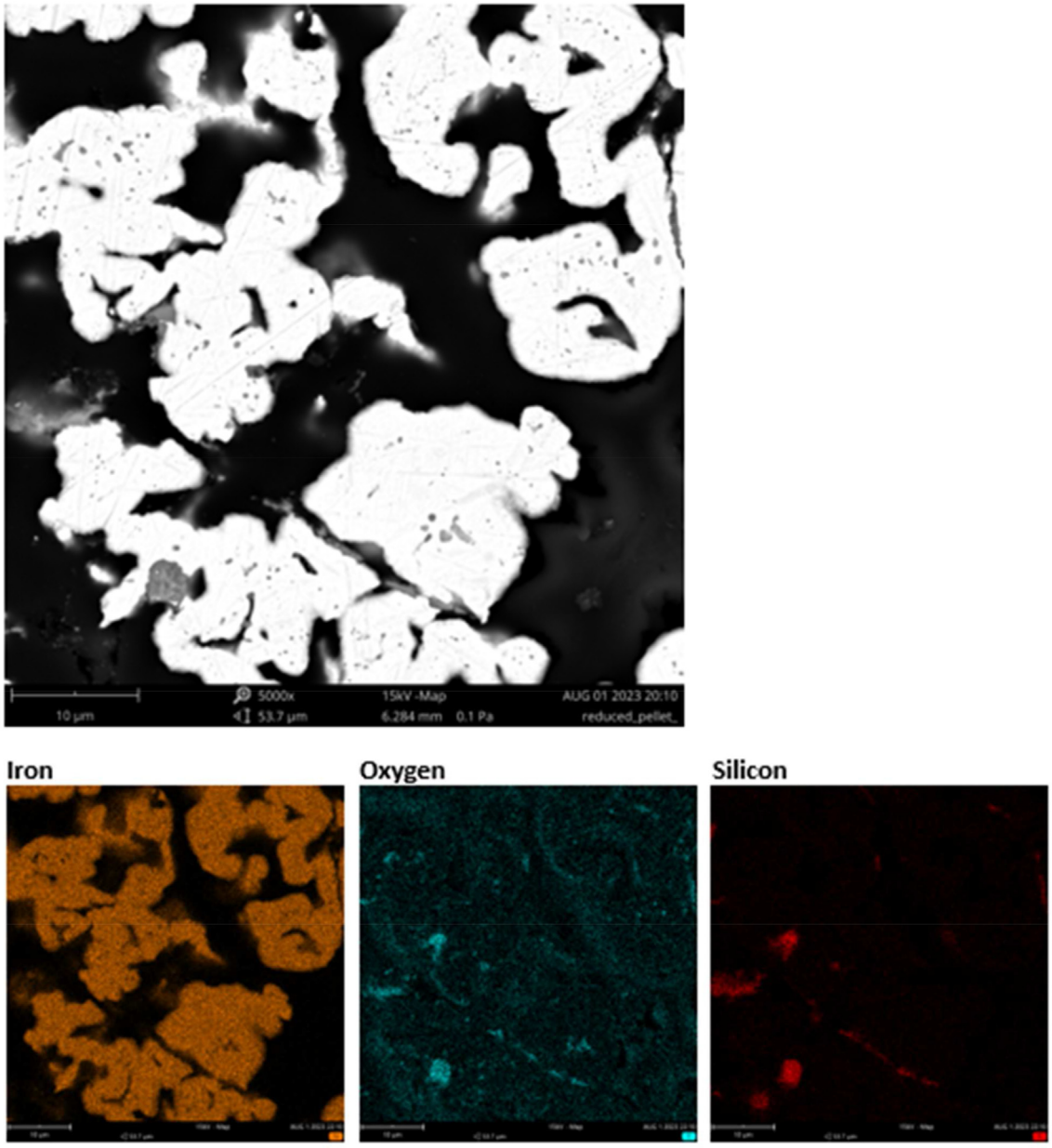

Fig. 19 – High magnification SEM and EDX maps of the reduced pellets.

Table 4 – Metallization behaviour of the pellets reduced in selected conditions.

Initial Weight	Moles of Fe2O3	Weight of O3	Weight of Fe2	Final Weight	Variation of weight	Temperature	Time	Remaining oxygen	Percentage of reduction
grams	moles	grams	grams	grams	grams	degree C	hours	grams	%
175,3338	1098	52,6001	122,73	125,4175	49,9163	850	1	2,68,384	95%
110,3406	0,691	33,1022	77,238	79,1142	31,2264	850	1,5	1,87,578	94%
110,0004	0,6888	33,0001	77	78,6818	31,3186	850	2	1,68,152	95%
110,1556	0,6898	33,0467	77,109	78,0259	32,1297	850	2,5	0,91,698	97%
110,7176	0,6933	33,2153	77,502	81,3718	29,3458	800	1	3,86,948	88%
110,6208	0,6927	33,1862	77,435	79,6846	30,9362	800	1,5	2,25,004	93%
110,4272	0,6915	33,1282	77,299	78,9868	31,4404	800	2	1,68,776	95%
110,372	0,6912	33,1116	77,26	78,1118	32,2602	800	2,5	0,8514	97%

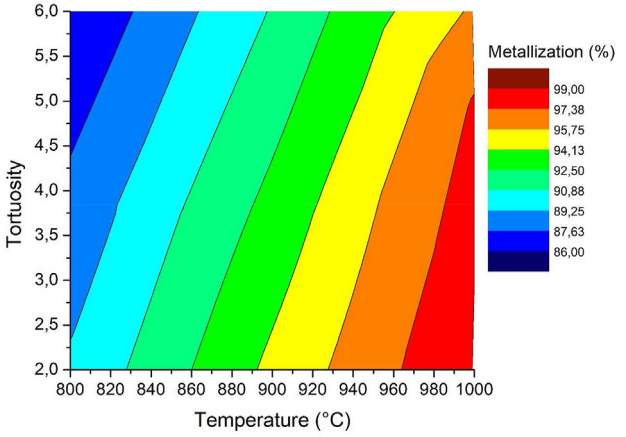

Fig. 20 – Metallization behaviour as a function of temperature and pores tortuosity.

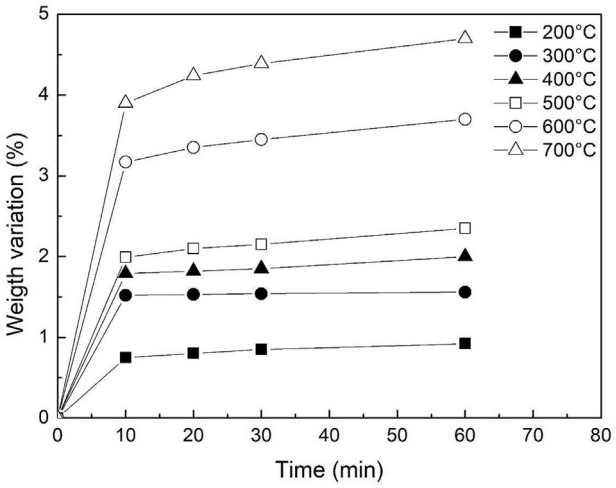

Fig. 21 – Weight variation of the pellets as a function of temperature and pressure (reoxidation curves refer to the pellets with larger diameter).

In all regions, the predominance of metallic Fe is observed. Despite the intense transformation, it is possible to identify the contours of the preceding oxide phase. The reduced pellet presents high porosity, being possible to distinguish intergranular porosity remnant of oxide particles and intragranular porosity generated from the transformation of the metallic Fe oxide.

The SEM/EDX analysis of the reduced sample's cross-section revealed a strong iron signal from inside the pellet. Similar to the pellets before the reduction process, silicon and oxygen were also detectable. Nevertheless, most of the oxygen signal comes from epoxy that was used for the cross-section preparation and from the same regions as silicon. It suggests that the silica phase remains in the pellet after the direct hydrogen reduction process. While in the sample before reduction, silica was detected between iron oxide particles (Fig. 19), after reduction in hydrogen, silica is mostly visible at the edges of iron particles. The reduced pellet presents high porosity, making it possible to distinguish between intergranular porosity remnant of oxide particles and intragranular porosity generated from the transformation of the metallic Fe oxide.

For some tested conditions, 800–850 °C in 100% hydrogen atmosphere the maximum metallization is close to 97% as shown in Table 4.

The metallization of the pellets depends on many different aspects. The main aspect (at a given temperature) influencing the metallization degree is the pores tortuosity. This is shown in Fig. 20.

So, pores geometry has the most remarkable effect on the pellets metallization behaviour as well as with the reduction temperature.

After reduction, the pellets were re-heated at different temperatures in order to evaluate the reoxidation behaviour. The results are shown in Fig. 21.

The extremely porous structure contributes to reoxidation reactions. Re-oxidation can take place through two distinct processes: corrosion in aqueous medium and air oxidation. While dry oxidation occurs slowly at low temperatures, the reaction in water vapour develops rapidly and can be considered as the cause of increased temperature to levels at which oxidation reactions at high temperatures begin to occur at high speeds and become self-sustaining. Most chemical reactions involving reoxidation of sponge iron are exothermic [61]. These reactions are limited in the case of carburized sponge iron because of the different porosity behaviour during reduction and because of the cementite formation leading to the material protection against rapid reoxidation [62]. In addition, some given conditions can lead to the rapid surface pores closure leading to a retardation of the carburized sponge iron [63].

Oxidation initially occurs at low temperatures through the reaction of metallic iron with humidity in the air:

$$2Fe + 3H_2O + 3O \leftrightarrow 2Fe(OH)_3$$

$$2Fe + H_2O + 3O \leftrightarrow 2FeOOH$$

These reactions are very exothermic and release an amount of heat that provides enough energy to enable the other oxidation reactions:

$$3Fe + 2O_2 \leftrightarrow Fe_3O_4$$

$$2Fe_3O_4 + \frac{1}{2}O_2 \leftrightarrow 2Fe_2O_3$$

$$Fe + \frac{1}{2}O_2 \leftrightarrow FeO$$

The last reaction takes place above 570 °C.

Oxidation does not occur isothermally in its first few steps stages since the reaction is exothermic and the heat released raises the temperature of the iron sponge significantly. They can be identified three stages of oxidation: (1) rapid initial –

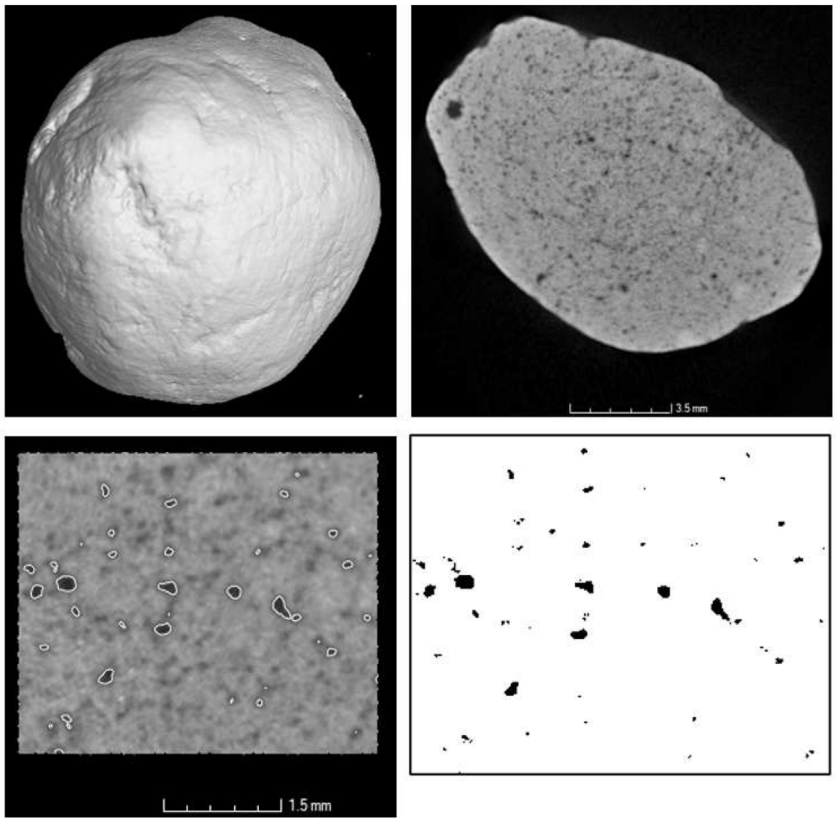

Fig. 22 – Microtomography aspect of the medium size pellet after reoxidation at 700 °C for 60 min.

characterized by a large slope of the curve; (2) intermediate - in which the oxidation rate decreases gradually; and (3) final - at a low, almost constant rate of oxidation even if the slope of the final stage tends to increase as the oxidation temperature increases. It was identified that the initial stages of reoxidation followed a linear equation, indicating then the chemical reactions at the interfaces as a controlling mechanism of the process. At the intermediate stage, the phenomenon follows a parabolic expression indicating diffusion in solid state. Finally, the final stages indicate a logarithmic relationship in the structure predominant, indicating that the controlling mechanism is solid state diffusion with formation of cavities at the interfaces between the oxide film and the metallic iron grains. One of the main reasons for this behaviour is due to the rapid reduction in porosity due to closure of the entrances to the interconnected network of pores during oxidation. A fraction of intragranular voids decreases (due to the difference in volume between metallic iron and their oxides) thus reducing the diffusion of the oxidizing gas, as well as the surface particle reactive. The rate of oxidation is then reduced due to the blockage of the non-porous oxide layers, when the inner grains become isolated from the network interconnected and the transport of reagents occurs only through diffusion in solid state.

The microtomography aspect of the medium size pellet after reoxidation at 700 °C for 60 min is shown in Fig. 22.

As observed, the aspect of the pellet is more similar to the one before reduction with a porosity close to 13%.

The SEM microstructure and the compositional map of the medium size pellets after reoxidation at 700 °C for 60 min is shown in Fig. 23.

The analyses of the samples show the dominant presence of metallic Fe in the reoxidized pellets. Even at higher magnifications, the dominance of iron and oxygen is clearly visible. Minority phases present in the samples were detected, such as Silicates or Ca-ferrites. The silicates regions were detected as separate areas at the edges of the iron oxide particles, similar to the pellets after the reduction process, and around the iron oxide particles, as for the raw pellet before reduction (Fig. 24).

The pellets showed a zoned structure due to the reoxidation process that occurs from the edge to the pellet core. The bulk is predominantly transformed into hematite. At the outer mantle, there is a narrow magnetite-wustite transition that is delimited by the Fe-metallic region. The Fe-metallic is still preserved in the core. Magnetite and wustite occur associated, with no marked discontinuities between the two phases.

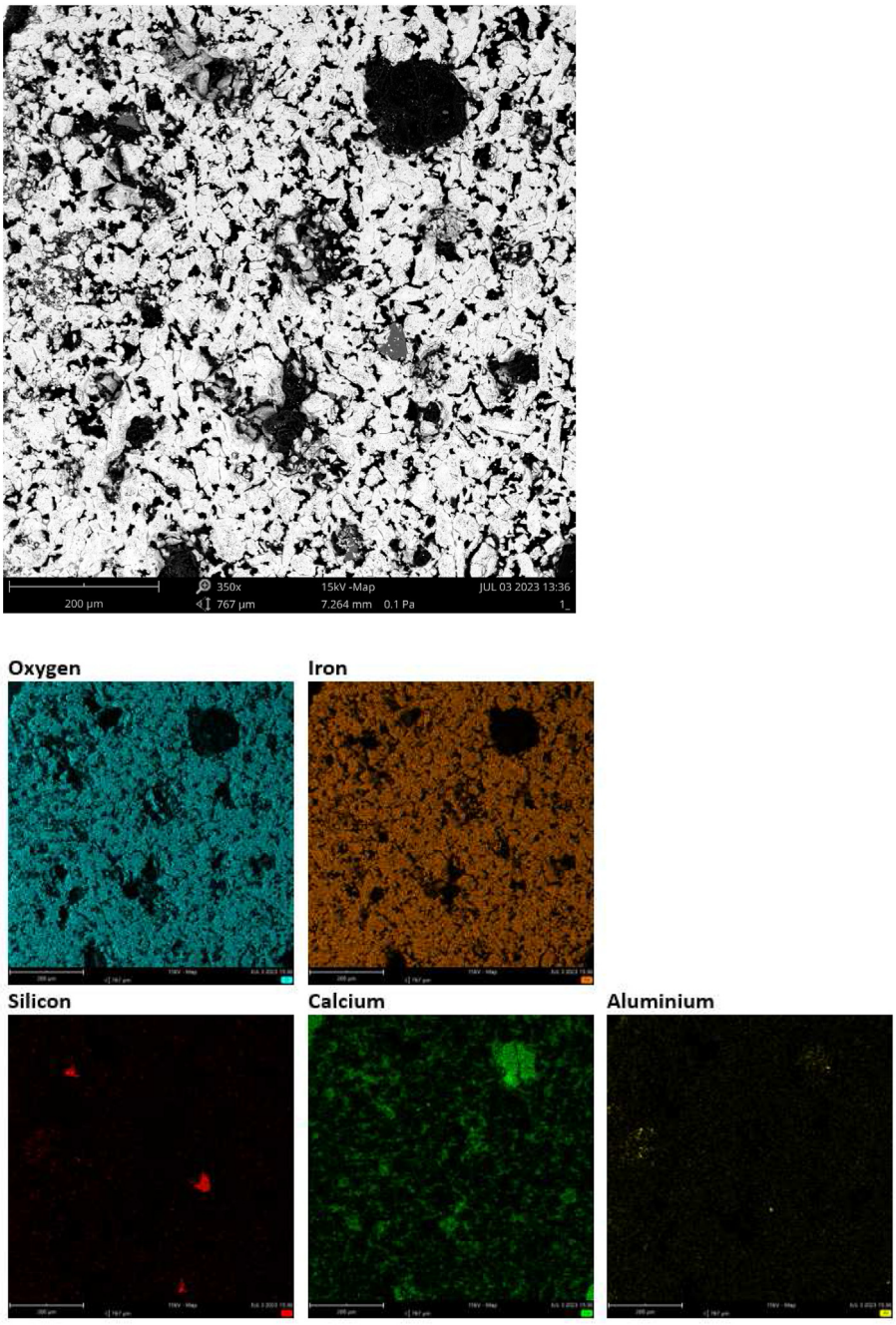

Fig. 23 – SEM microstructure and compositional map of the medium size pellet reoxidized at 700 °C for 60 min.

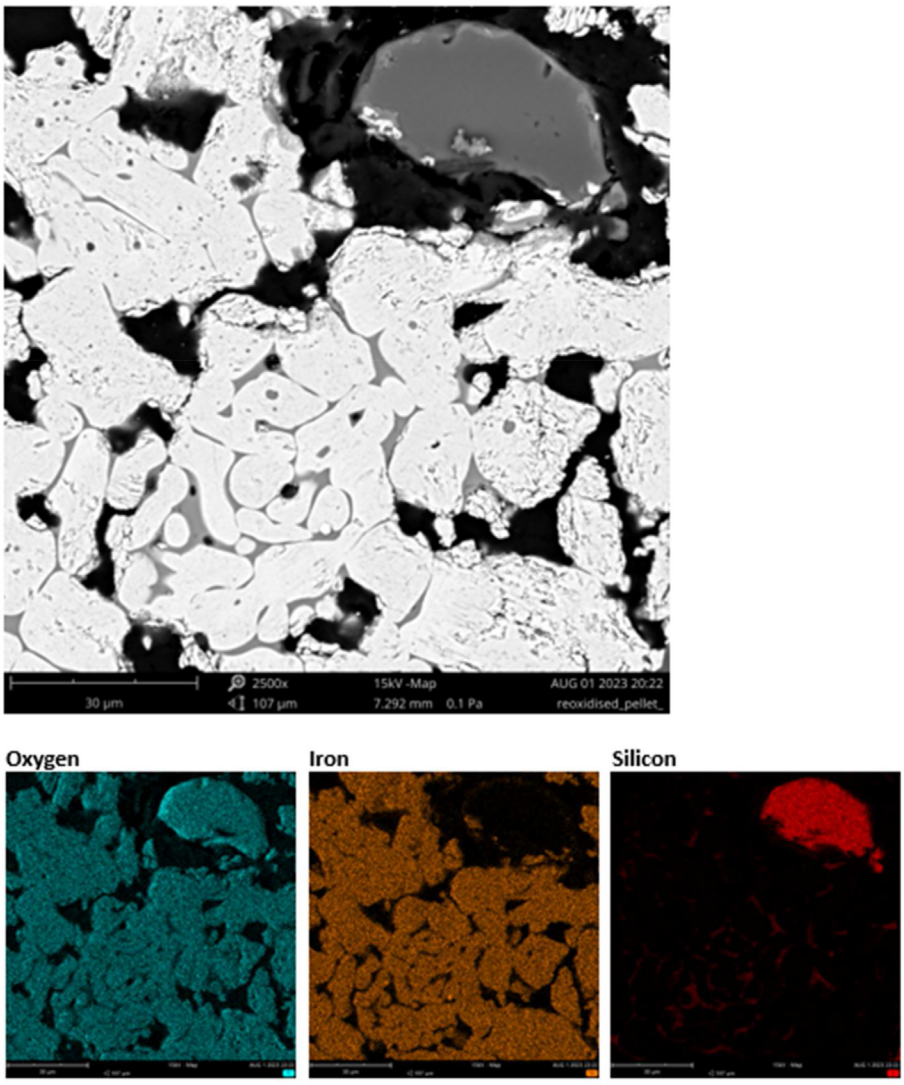

Fig. 24 – High magnification SEM and EDX maps of the reoxidized pellets.

4. Conclusions

Given all the observations performed on high-grade pellets reduced in hydrogen atmosphere and re-oxidized at different temperatures many conclusions can be taken. Pellets were reduced in hydrogen atmosphere at 8 bar in the temperature range 800–1000 °C. The reduction behaviour was monitored through microtomography mapping of the pellets showing a remarkable increase of the porosity as the pellets go toward complete metallization. Also, the pores dimensions and the pores tortuosity led to an increase as the hydrogen direct reduction proceeds. It was demonstrated how tortuosity of the pores largely decelerate the kinetic behaviour of the pellets because of the increase of the flowing gas turbulence inside the pellets bulk. Given that the tortuosity tends to increase during the reduction, a pronounced increase of the tortuosity tends to retard the kinetic of the reduction reactions. After reduction, the pellets were re-oxidized in the temperature range 200–700 °C. A very slow weight increase was recorded for temperatures below 500 °C. For higher temperatures the reoxidation results faster and faster with a weight increase of 4% after 10 min of exposure to 700 °C in air.

Declaration of competing interest

The authors declare that they have no known competing financial interests or personal relationships that could have appeared to influence the work reported in this paper.

Acknowledgments

Authors would like to thank the Italian Ministry for University and Research (MUR) for the fundings provided under the Grant "Low environmental impact fuels for metallurgical industries-2022P3PJXN".

REFERENCES

[1] Cavaliere P. Blast furnace: most efficient technologies for greenhouse emissions abatement. In: Clean ironmaking and steelmaking processes. Cham: Springer; 2019.
[2] Cavaliere P. Direct reduced iron: most efficient technologies for greenhouse emissions abatement. In: Clean ironmaking and steelmaking processes. Cham: Springer; 2019.
[3] Vokhmyakov IS, Bersenev IS, Borodin AV, Stepanova AA, Zagainov SA, Gileva lY. Mechanism of oxidation for hot briquetting iron (HBI). Steel Transl 2022;52:331–6.
[4] Li Jiayuan, Liang Zhikai, Yi Lingyun, Huang Boyang, Chen Jun, Han Hetong, Huang Zhucheng. Novel insights into the reoxidation of direct reduced iron (DRI) during ball-mill treatment: a combined experimental and computational study. Appl Surf Sci 2021;552:149485.
[5] Yazir D, Sahin B, Alkac M. Selection of an inert gas system for the transportation of direct reduced iron. Math Probl Eng 2021:8529724.
[6] Hamadeh H, Mirgaux O, Patisson F. Detailed modeling of the direct reduction of iron ore in a shaft furnace. Materials 2018;11(10):1865.
[7] Anameric B, Kawatra K. Properties and features of direct reduced iron. Miner Process Extr Metall Rev 2007;28(1):59–116.
[8] Zang G, Sun P, Elgowainy A, Bobba P, McMillan C, Ma O, Podkaminer K, Rustagi N, Melaina M, Koleva M. Cost and life cycle analysis for deep CO2 emissions reduction for steel making: direct reduced iron technologies. Steel Res Int 2023;94(6):2200297.
[9] Pfeiffer A, Ernst D, Zheng H, Wimmer G, Schenk J. The behavior of direct reduced iron in the electric arc furnace hotspot. Metals 2023;13(5):978.
[10] Meshram A, Govro J, Omalley RJ, Sridhar S, Korobeinikov Y. Modeling isothermal reduction of iron ore pellet using finite element analysis method: experiments & validation. Metals 2022;12(12):2026.
[11] Cavaliere P, Perrone A, Marsano D. Effect of reducing atmosphere on the direct reduction of iron oxides pellets. Powder Technol 2023;426:118650.
[12] Cavaliere P, Perrone A, Marsano D. Critical analysis of variable atmosphere gaseous reduction of iron oxides pellets. Ironmak Steelmak https://doi.org/10.1080/03019233.2023.2194732.
[13] Cavaliere P, Perrone A, Marsano D, Primavera V. Hydrogen-based direct reduction of iron oxides pellets modeling. Steel Res Int 2023;94(6):2200791.
[14] Cao Z, Xu Q, Kang H, Shi J, Lu X, Chen B, Guo L. Insights into direct reduction iron using bamboo biomass as a green and renewable reducer: reduction behavior study and kinetics analysis. Sci Total Environ 2023:880. 163393.
[15] Dutta SK, Sah R. Worldwide direct reduced iron scenario and hazards associated with their storage and shipments. Iron Ore Pellet 2014;58(4).
[16] Bandopadhyay A, Ganguly A, Gupta KN, Ray HS. Investigations on the anomalous oxidation behaviour of high-carbon gas-based direct reduced iron (DRI). Thermochim Acta 1996;276:199–207.
[17] AbdElmomen SS. Reoxidation of direct reduced iron in ambient air. Ironmak Steelmak 2014;41(2):107–11.
[18] Milandia A, Juniarsih A, Muadz R, Sactianto A, Suryana. The effect of heat energy on/of iron direct reduction process. IOP Conf Ser Mater Sci Eng 2019;673:012137.
[19] Durnovich D, Miller T. The basic of DRI plant safety. Direct form midrex sept; 2019.
[20] Godoy MP. Carbon formation in direct reduced iron and hot briquetted iron. Colorado School of Mines; 2020.
[21] Saidi A, Izadi J, Safarian J. Characterization of re-oxidation behavior of sponge iron produced from different type of iron ore. In: SCANMET II – 2nd international conference on process development in iron and steelmaking. Suécia: Lulea; 2004. p. 285–93.
[22] Cavaliere P. Electric Arc furnace: most efficient technologies for greenhouse emissions abatement. In: Clean ironmaking and steelmaking processes. Cham: Springer; 2019.
[23] Li Shaofei, Gu Huazhi, Huang Ao, Zou Yongshun, Yang Shuang, Fu Lvping. Thermodynamic analysis and experimental verification of the direct reduction of iron ores with hydrogen at elevated temperature. J Mater Sci 2022;57:20419–34.
[24] Li Yanjun, Li Peiyu, Yu Jianwen, Han Yuexin, Gao Peng. Effect of temperature on reduction behaviors and microstructural changes of magnetite with H2 under fluidized bed conditions. Steel Res Int 2022;93(7):2100749.
[25] Zare Ghadi Ariyan, Radfar Navid, Sadegh Valipour Mohammad, Sohn Hong Yong. A review on the modeling of direct reduction of iron oxides in gas-based shaft furnaces. Steel Res Int 2023;94(6):2200742.
[26] Abd Elmomen SS. Reoxidation of direct reduced iron in stagnant air in the temperature range between 150 and 450°C. The bulletin of Tabbin Institute for Metallurgical studies 2021; 109(1):72–86. https://doi.org/10.21608/TIMS.2021.191719.
[27] Ünal HI, Turgut E, Atapek SH, Alkan A. Direct reduction of ferrous oxides to form an iron-rich alternative charge material. High Temp Mater Process 2015;34(8):751–6.
[28] Cavaliere P. Hydrogen direct reduced iron. In: Hydrogen assisted direct reduction of iron oxides. Cham: Springer; 2022.
[29] Fradet Q, Ali ML, Riedel U. Development of a porous solid model for the direct reduction of iron ore pellets. Steel Res Int 2022;93(12):2200042.
[30] Rechberger K, Spanlang A, Conde AS, Wolfmeir H, Harris C. Green hydrogen-based direct reduction for low-carbon steelmaking. Steel Res Int 2020;91(11):2000110.
[31] Cavaliere P. Hydrogen in reduction processes. In: Hydrogen assisted direct reduction of iron oxides. Cham: Springer; 2022.
[32] Li P, Li Y, Yu J, Gao P, Han Y. Kinetics and microstructural changes during fluidized reduction of magnetite with hydrogen at low temperatures. Int J Hydrogen Energy 2022;47(73):31140–51.
[33] Hjortsberg E, Forsberg F, Gustafsson G, Rutqvist E. X-ray microtomography for characterisation of cracks in iron ore pellets after reduction. Ironmak Steelmak 2013;40(6):399–406.
[34] Soares Augusto K, Paciornik S. Porosity characterization of iron ore pellets by X-ray microtomography. Mat Res 2018;21(2).
[35] Bam LC, Miller JA, Becker M, Basson IJ. X-ray computed tomography: practical evaluation of beam hardening in iron ore samples. Miner Eng 2019;131:206–15.
[36] Ma Y, Souza FilhoIR, Bai Y, Schenk J, Patisson F, Beck A, van Bokhoven JA, Willinger MG, Li K, Xie D, Ponge D, Zaefferer S, Gault B, Mianroodi JR, Raabe D. Hierarchical nature of hydrogen-based direct reduction of iron oxides. Scripta Mater 2022;213:114571.
[37] Lemus J, Mendoza G, Bedolla E. Reoxidation and carburization study of reduced iron ore pellets. Rev Metal (Madr) 1998;34(6):459–68.
[38] Zhao Zichuan, Tang Jue, Chu Mansheng, Wang Xindong, Zheng Aijun, Wang Xiaoai, Yang Li. Direct reduction swelling behavior of pellets in hydrogen-based shaft furnaces under typical atmospheres. Int J Miner Metall Mater 2022;29:1891–900.
[39] Cavalcanti PP, Tavares LM. Statistical analysis of fracture characteristics of industrial iron ore pellets. Powder Technol

2018;325:659–68. https://doi.org/10.1016/j.powtec.2017.11.062.
[40] Cavaliere P, Perrone A, Dijon L, Laska A, Koszelow D. Direct reduction of pellets through hydrogen: experimental and model behaviour, submitted to Int J Hydrogen Energy (The article is under review).
[41] Metolina P, Ramos Ribeiro T, Guardani R. Hydrogen-based direct reduction of industrial iron ore pellets. Int J Miner Metall Mater 2022;29:1908–21.
[42] Bhuiyan IU, Mouzon J, Forsberg F, Forsmo SPE, Sjödahl M, Hedlund J. Consideration of X-ray microtomography to quantitatively determine the size distribution of bubble cavities in iron ore pellets. Powder Technol 2013;233:312–8.
[43] Moreira AC, Appoloni CR, Mantovani IF, Fernandes JS, Marques LC, Nagata R, Fernandes CP. Effects of manual threshold setting on image analysis results of a sandstone sample structural characterization by X-ray microtomography. Appl Radiat Isot 2012;70(6):937–41.
[44] Álvarez Iglesias JC, Soares Augusto K, da Fonseca Martins Gomes O, Leite Alcântara Domingues A, Vieira MB, Casagrande C, Paciornik S. Automatic characterization of iron ore by digital microscopy and image analysis. J Mater Res Technol 2018;7(3):376–80. https://doi.org/10.1016/j.jmrt.2018.06.014.
[45] Augusto KS, Alves H, Mauricio MHP, Paciornik S. 3D characterization of iron ore pellets by XrayMicroCT. 14th International Congress for Stereology and Image Analysis Liège, July 7-10. 2015.
[46] Zheng X, Paul S, Moghimi L, Wang Y, Vilá RA, Zhang F, Gao X, Deng J, Jiang Y, Xiao X, Wu C, Greenburg LC, Yufei Yang, Cui Y, Vailionis A, Kuzmenko I, llavsky J, Yin Y, Cui Y, Dresselhaus-Marais L. Correlating chemical reaction and mass transport in hydrogen-based direct reduction of iron oxide. https://doi.org/10.48550/arXiv.2302.14215.
[47] Heidari A, Niknahad N, Iljana M, Fabritius T. A review on the kinetics of iron ore reduction by hydrogen. Materials 2021;14(24):7540.
[48] Wang R, Zhao Y, Babich A, Senk D, Fan X. Comprehensive study on the reduction of biomass embedded self-reducing pellets (SRP) under H2 involved conditions by TG-DTA. Powder Technol 2022;407:117654.
[49] Guo D, Hu M, Pu C, Xiao B, Hu Z, Liu S, Wang X, Zhu X. Kinetics and mechanisms of direct reduction of iron ore-biomass composite pellets with hydrogen gas. Int J Hydrogen Energy 2015;40(14):4733–40.
[50] Mirzajani A, Ebrahim H, Nouri SMM. Simulation of a direct reduction moving bed reactor using a three interface model. Braz J Chem Eng 2018;35(3):1019–28.
[51] Chai Yifan, Fan Yingjie, Li Zhichao, Wu Jiayi, Zhang Yunhao, Wang Yici, Luo Guoping, An Shengli. Kinetics of reduction in stages of pellets prepared from the bayan obo iron ore concentrate. ACS Omega 2022;7(9):7759–68.
[52] Murakami T, Wakabayashi H, Maruoka D, Kasai E. Effect of hydrogen concentration in reducing gas on the changes in mineral phases during reduction of iron ore sinter. ISIJ Int 2020;60(12):2678–85.
[53] Spreitzer D, Schenk J. Reduction of iron oxides with hydrogen—a review. Steel Res Int 2019;90(10):1900108.
[54] Ali ML, Fradet Q, Riedel U. Kinetic mechanism development for the direct reduction of single hematite pellets in H2/CO atmospheres. Steel Res Int 2022;93(12):2200043.
[55] Bonalde A, Enriquez A, Manrique M. Kinetic analysis of the iron oxide reduction using hydrogen-carbon monoxide mixtures as reducing agent. ISIJ Int 2005;45(9):1255–60.
[56] Zare Ghadi A, Valipour MS, Biglari M. Transient entropy generation analysis during wustite pellet reduction to sponge iron. IJE Trans B: Appl 2018;31(8):1274–82.
[57] Kim SH, Zhang X, Ma Y, Souza Filho IR, Schweinar K, Angenendt K, Vogel D, Stephenson LT, El-Zoka AA, Rezaei Mianroodi J, Rohwerder M, Gaulta B, Raabe D. Influence of microstructure and atomic-scale chemistry on the direct reduction of iron ore with hydrogen at 700°C. Acta Mater 2021;212:116933.
[58] Sundberg R. Reduction of iron oxides with hydrogen, master degree thesis. Abo Akademy University; 2021.
[59] Zhang Guo-Cheng, Luo Guo-Ping, Jia Peng-Fei, Wang Yi-Ci, Chai Yi-Fan. Effect of basicity on the reduction swelling properties of iron ore briquettes. High Temp Mater Process 2021;40:193–203.
[60] Shi Yue, Zhu Deqing, Pan Jian, Guo Zhengqi, Lu Shenghu, Xu Mengjie. Improving hydrogen-rich gas-based shaft furnace direct reduction of fired hematite pellets by modifying basicity. Powder Technol 2022;408:117782.
[61] Sharma PK, Rajput NS, Jain S. Reoxidation of sponge iron in an exothermic process due to removal of hydrogen. Int J Adv Res Sci Eng 2012;1(1).
[62] Herbig C, Brender A, Jess A. Reoxidation and ignition of iron and sponge iron. Part II: production of non-pyrophoric sponge iron by reduction and carburization in a fluidized bed reactor. Steel Grips 2003;1:200–5.
[63] Paknahad P, Askari M. Modeling, kinetics investigation and determining the controlling mechanisms of atmospheric oxidation of "cold briquetted iron and carbon (CBIC)". Metall Eng 2020;23(3):206–19.